Originally published as:

Schäppi, R., Rutz, D., Dähler, F., Muroyama, A., Haueter, P., Lilliestam, J., Patt, A., Furler, P., Steinfeld, A. (2022): Drop-in Fuels from Sunlight and Air. - Nature, 601, 63-68.

DOI: https://doi.org/10.1038/s41586-021-04174-y

Preprint version of the article: Schäppi, R., Rutz, D., Dähler, F., Muroyama, A., Haueter, P., Lilliestam, J., Patt, A., Furler, P., Steinfeld, A. (2022): Drop-in fuels from sunlight and air, in Nature 601, pp. 63-68. https://doi.org/10.1038/s41586-021-04174-y.

Drop-in fuels from sunlight and air

Remo Schäppi[1], David Rutz[1], Fabian Dähler[1], Alexander Muroyama[1], Philipp Haueter[1], Johan Lilliestam[2,3], Anthony Patt[4], Philipp Furler[1,5*], Aldo Steinfeld[1*]

[1] Department of Mechanical and Process Engineering, ETH Zürich, 8092 Zürich, Switzerland

[2] Institute for Advanced Sustainability Studies (IASS), 14467 Potsdam, Germany

[3] University of Potsdam, Faculty of Economics and Social Sciences, 14482 Potsdam, Germany

[4] Department of Environmental Systems Science, ETH Zürich, 8092 Zürich, Switzerland

[5] Synhelion SA, 6900 Lugano, Switzerland

[*]Corresponding authors: philipp.furler@synhelion.com, aldo.steinfeld@ethz.ch

Aviation and shipping currently contribute approximately 8% of total anthropogenic CO_2 emissions, with growth in tourism and global trade projected to increase this contribution further[1-3]. Carbon-neutral transportation is feasible with electric motors powered by rechargeable batteries, though challenging if not impossible for long-haul commercial travel, particularly air travel[4]. A promising solution are drop-in fuels (synthetic alternatives for petroleum-derived liquid hydrocarbon fuels such as kerosene, gasoline or diesel) made from H_2O and CO_2 by solar-driven processes[5-7]. Among the many possible approaches, the thermochemical path using concentrated solar radiation as the source of high-temperature process heat offers potentially high production rates and efficiencies[8] and can deliver truly carbon-neutral fuels if the required CO_2 is obtained directly from atmospheric air[9]. If H_2O is also co-extracted from air[10], feedstock sourcing and fuel production can be co-located in desert regions with high solar irradiation and limited access to water resources. While individual steps of such a scheme have been implemented, we now demonstrate operation of the entire thermochemical solar fuel production chain, from H_2O and CO_2 captured directly from ambient air to the synthesis of drop-in transportation fuels (e.g. methanol, kerosene), with a modular 5-$kW_{thermal}$ pilot-scale solar system operated under real field conditions. We further identify the R&D efforts and discuss the economic viability and policies required to bring these solar fuels to market.

Solar fuel production using H_2O and CO_2 obtained through direct air capture (DAC) has so far largely been limited to bench-top[11,12] or pilot-scale[13,14] demonstrations of individual steps. A combined PV-electrolysis system[15] produced solar fuels from water and captured CO_2, but the set-up was not optimized and coupling of intermittent solar hydrogen production with continuous non-solar hydrocarbon synthesis necessitated the co-feeding of fossil-derived syngas.

The solar fuel system

Figure 1 sketches our solar fuel system, located on the roof of the ETH's Machine Laboratory Building in Zurich. Its three essential units are: 1) the direct air capture (DAC) unit which co-extracts CO_2 and H_2O directly from ambient air; 2) the solar redox unit which converts CO_2 and H_2O into a desired mixture of CO and H_2 (syngas); and 3) the gas-to-liquid (GTL) unit which converts syngas to liquid hydrocarbons or methanol. Technical details are presented in Methods.

Preprint version of the article: Schäppi, R., Rutz, D., Dähler, F., Muroyama, A., Haueter, P., Lilliestam, J., Patt, A., Furler, P., Steinfeld, A. (2022): Drop-in fuels from sunlight and air, in Nature 601, pp. 63-68. https://doi.org/10.1038/s41586-021-04174-y.

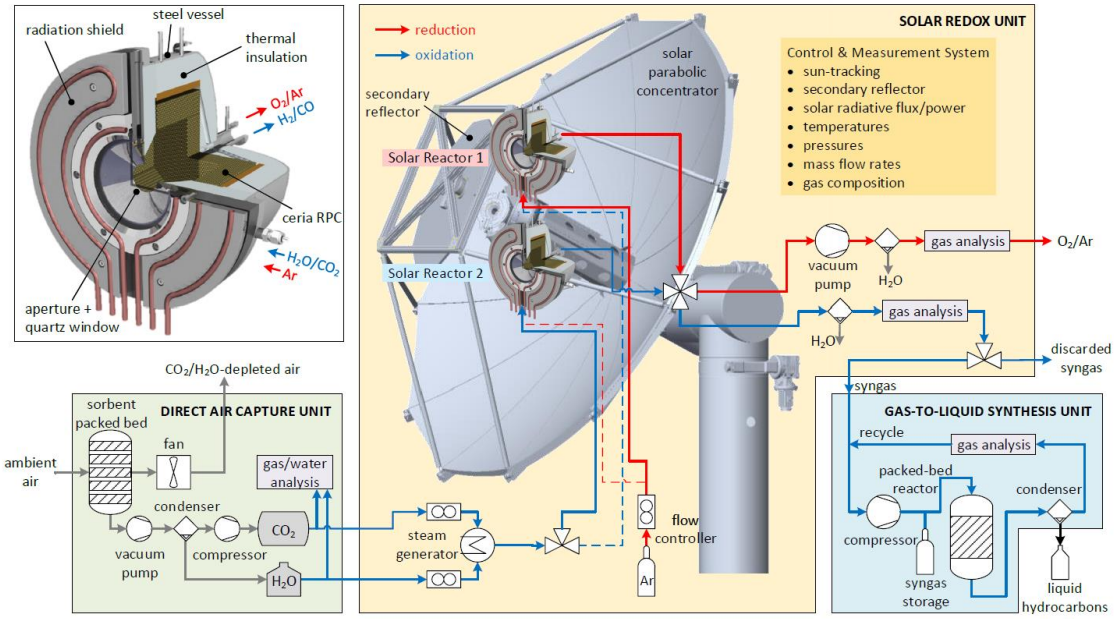

Figure 1. Simplified process chain of the solar fuel system integrating three thermochemical conversion units in series: 1) the direct air capture (DAC) unit which co-extracts CO_2 and H_2O directly from ambient air; 2) the solar redox unit which converts CO_2 and H_2O into a desired mixture of CO and H_2 (syngas) using concentrated solar energy; and 3) the gas-to-liquid (GTL) synthesis unit which finally converts syngas to methanol or liquid hydrocarbons. Two identical solar reactors are positioned at the focus of the solar concentrator for performing both redox steps of the thermochemical cycle simultaneously by alternating the concentrated solar input between them. While one solar reactor is performing the endothermic reduction step on sun, the second solar reactor is performing the exothermic oxidation step off sun. Red arrow indicates reduction (Eq. 1); blue arrow indicates oxidation (Eq. 2/3). Dimensions are not to scale. *Upper-left insert*: Cross-section of the solar reactor featuring a cavity-receiver containing a reticulated porous ceramic structure (RPC) made of pure ceria for performing the thermochemical redox cycle.

The DAC unit, commercialized by the ETH's spinoff Climeworks, applies adsorption-desorption cycles to an amine-functionalized sorbent to concurrently extract CO_2 and H_2O from ambient air[10]. Adsorption proceeds at ambient temperature and pressure for 180 minutes per cycle, desorption at 95°C and 0.1-0.3 bar for 43 minutes per cycle. The unit can process an air flow of 2000 m^3/hr with 5.5 cycles/day, yielding around 8 kg/day of CO_2 with a measured purity of 98% (the remainder being air) and 20-40 kg/day of water (depending on air relative humidity) with contaminants below the 0.2 ppm detection limit. The exhaust air leaves the unit during the adsorption step with about 40-70% of its initial CO_2 content captured. The captured CO_2 stream exiting the DAC unit during the desorption step is collected in a balloon-type buffer reservoir at ambient pressure and subsequently compressed to maximum 12 bars and stored in a 750 l steel buffer tank. Water is condensed out of the desorption stream and stored in a plastic buffer tank. Both CO_2 and H_2O are delivered from their buffer tanks to the solar redox unit according to demand.

The solar redox unit produces CO and H_2 through thermochemical splitting of CO_2 and H_2O via a reduction-oxidation (redox) cycle driven by concentrated solar radiation[8]. We use nonstoichiometric ceria ($CeO_{2-\delta}$) as redox material because of its rapid kinetics, crystallographic stability, and abundance[16,17]. Alternative redox materials, e.g. perovskites[18-19] and hercynite[20], may exhibit superior redox performance but have not yet proven to be as stable as ceria. The redox cycle at the heart of the solar redox unit comprises two steps. In

the first endothermic step, ceria is thermally reduced to generate O_2 (Methods, Eq. 1). In the second exothermic step, the reduced ceria is re-oxidized with CO_2 and/or H_2O to generate CO and/or H_2, respectively (Methods, Eq. 2 and 3). Ceria is thus not consumed and the net overall reactions are CO_2=CO+½O_2 and H_2O=H_2+½O_2, but with the fuel (H_2, CO) and O_2 generated in separate steps and thus avoiding the formation of explosive mixtures and obviating the need for high-temperature gas separation. The thermochemical redox cycle based on non-stoichiometric ceria ($CeO_{2-\delta}$) is represented by the following reactions and the corresponding standard enthalpy changes:

Reduction:

$$\frac{1}{\Delta\delta} CeO_{2-\delta_{ox}} \rightarrow \frac{1}{\Delta\delta} CeO_{2-\delta_{red}} + \frac{1}{2} O_2 \qquad \Delta H° \approx 475 \text{ kJ per ½ mole } O_2 \qquad (1)$$

Oxidation with CO_2:

$$\frac{1}{\Delta\delta} CeO_{2-\delta_{red}} + CO_2 \rightarrow \frac{1}{\Delta\delta} CeO_{2-\delta_{ox}} + CO \qquad \Delta H° \approx \text{-192 kJ/mol } CO_2 \qquad (2)$$

Oxidation with H_2O:

$$\frac{1}{\Delta\delta} CeO_{2-\delta_{red}} + H_2O \rightarrow \frac{1}{\Delta\delta} CeO_{2-\delta_{ox}} + H_2 \qquad \Delta H° \approx \text{- 234 kJ/mol } H_2 \qquad (3)$$

δ denotes the non-stoichiometry – the measure of the redox extent which, in equilibrium, is a function of temperature and oxygen partial pressure. In principle, the redox cycle can be operated under a temperature-swing mode and/or a pressure-swing mode to control the oxygen exchange capacity of ceria $\Delta\delta = \delta_{red}$-$\delta_{ox}$, and thereby the fuel yield per cycle. Isothermal operation, i.e. only pressure-swing mode, suffers from low $\Delta\delta$ imposed by the thermodynamics[21-25]. For example, isothermal cycling at $T_{reduction} = T_{oxidation}$ = 1200°C with a pressure swing between 0.1 mbar and 1 bar, yields only $\Delta\delta$ = 0.003. We apply a combination of both temperature and pressure swing modes to maximize the oxygen exchange capacity of ceria, and thereby the fuel yield per cycle. For typical operating conditions of the reduction step at 1500°C and 0.1 mbar and the oxidation step at 900°C and 1 bar, thermodynamic predicts an order of magnitude higher value, $\Delta\delta$ = 0.04.

The solar reactor development evolved from its early design with monolithic ceria[24] to its present configuration with reticulated structures[25]. As sketched in Figure 1 (insert), it consists of a cavity-receiver with a circular aperture sealed by a quartz window for the access of concentrated solar radiation (apparent absorptivity = 0.99). The cavity contains a reticulated porous ceramic (RPC) structure made of ceria with dual-scale interconnected porosity in the mm and μm ranges for enhanced heat and mass transfer[26]. Since only the endothermic reduction step requires a solar input, we employ two identical solar reactors and perform both redox steps simultaneously by alternating the concentrated solar input between them. The required alternation of the solar concentrator focus is enabled by using a primary sun-tracking paraboloidal concentrator coupled to a secondary planar rotating reflector[27] (scheme in Fig. 1, photograph in Extended Data Fig. 1). For a direct normal solar irradiation (DNI) of 1 kW/m^2, the solar concentrator delivers alternately a solar radiative power up to 7.7 $kW_{thermal}$ at a peak flux concentration of 5,010 suns and an average flux of 2,710 suns measured over the 30 mm-radius aperture of each solar reactor.

The solar redox unit can split pure CO_2, pure H_2O, and both H_2O and CO_2 simultaneously. A purge gas (Ar or air) guides the fluid flow during the reduction step performed under vacuum pressures. Additionally, when co-splitting H_2O and CO_2 simultaneously, Ar or CO_2 (depending on the targeted syngas composition) is injected after the reduction step to re-pressurize the cavity prior to the oxidation step. The consumption of inert gas introduces an energy penalty and, consequently, affects detrimentally the system efficiency, but

its use can be avoided (Methods). Figure 2 shows a representative 7-hour day run with 17 consecutive redox cycles for co-splitting H_2O and CO_2, yielding 96.2 L (standard liters, including all species H_2, CO, CO_2, and Ar) of syngas with composition 59.5% H_2, 4.6% CO, 17.5% CO_2, and 18.4% Ar. The oxygen mass balance confirmed total selectivity for the conversion of H_2O to H_2 and of CO_2 to CO. The daily mass specific yield of syngas was 12.81 L/kg of ceria and its cumulative molar ratio H_2:CO_x was 2.7. The cumulative CO_2-to-CO molar conversion was 15.1%; a peak value of 65% was obtained for CO_2 splitting only[25]. This conversion can be further increased by reducing the CO_2 mass flow rate but at the expense of producing less syngas. The presence of unreacted CO_2 in the syngas obviously affects its molar ratio H_2:CO_x, which is critical for methanol synthesis but less relevant for Fischer-Tropsch (FT) synthesis. In the run on this specific day, the targeted syngas quality was the one suitable for methanol synthesis. As the DNI varied with time, the inlet gas flows were adjusted to match the duration of the reduction step with that of the oxidation step, enabling the switching of the solar input between the two solar reactors without delay and, thus, making continuous use of the solar input. Extended Data Figs. 4 and 5 show the syngas composition and yield as well as the cyclic variation and cumulative molar ratio H_2:CO_x for 152 consecutive redox cycles, yielding 1069.7 L of syngas with composition 58.4% H_2 , 5% CO, 18.6% CO_2 and 18% Ar (after condensation of unreacted water) and with a cumulative molar ratio H_2:CO_x = 2.48. This solar syngas was further processed to methanol in the GTL unit.

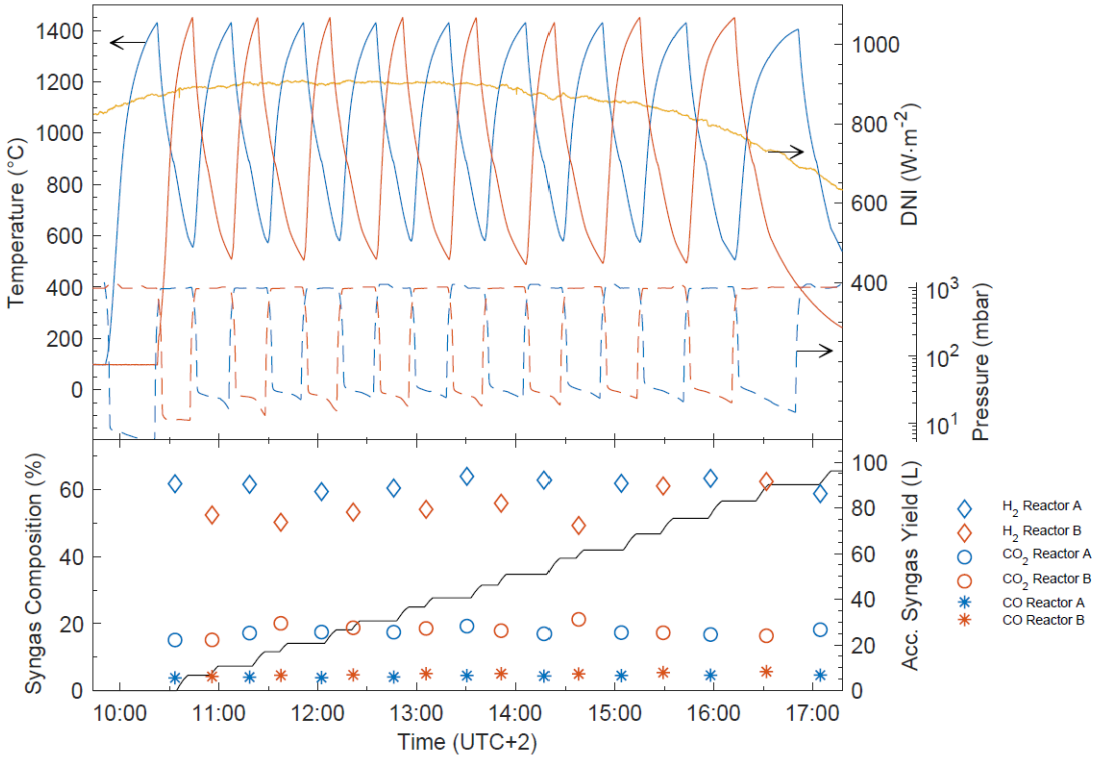

Figure 2. Representative day run of the solar redox unit for co-splitting H_2O and CO_2. Temporal variations of the direct normal solar irradiation (DNI), temperature, pressure, syngas composition, and cumulative syngas yield of the two adjacent solar reactors A and B (blue and red curves, respectively) performing the thermochemical redox cycle simultaneously. The concentrated solar radiative input is alternated between the solar reactors A and B: while one reactor is solar irradiated to effect the reduction step (Eq. 1), H_2O and CO_2 are injected in the second reactor to effect the oxidation step (Eq. 2/3). Inlet mass flow rates: 0.5 L/min Ar during reduction; 0.3 L/min CO_2 and 9.8 g/min H_2O during oxidation. L denotes standard liters.

Downstream of the solar redox unit (Fig. 1), the O_2 stream evolving from the reduction step is analyzed and vented. The syngas stream evolving from the oxidation step is analyzed and sent to the GTL unit, where it is first compressed for storage in a 5-liter buffer gas cylinder at up to 250 bar. The final syngas processing to methanol is a mature technology and uses a commercial Cu-ZnO-Al_2O_3 catalyst (Product No. 45776, Alfa Aesar) in a packed-bed tubular reactor at 230 °C and 50 bars. The measured single-pass molar conversion of the GTL unit was 27%, yielding methanol with a purity of 65%, the rest being water (contaminants below the detection limit, e.g. ethanol and butanol < 1 ppm, propanol < 10 ppm). The remaining unconverted syngas was recycled for multiple passes through the GTL unit. However, since Ar concentration increased with each pass, the recycled syngas was discarded after 6 consecutive passes, resulting in a total molar conversion of 85%. For example, for the representative 7-hour day run of Fig. 2, the amount of pure methanol produced was 3.2 cl.

Depending on the catalyst used in the GTL unit, the desired H_2:CO_x molar ratio of syngas for methanol synthesis lies between 2 and 3, while the desired H_2:CO molar ratio of syngas for FT synthesis is about 2. The syngas composition, especially the molar ratios H_2:CO and CO:CO_2, can be controlled by adjusting the H_2O:CO_2 feed ratio to the solar reactor[28] and/or by performing separately the splitting of CO_2 and H_2O[24,25,29] and/or by simply choosing appropriate start and end times of the syngas collection. In either case, the syngas purity and quality is suitable for GTL processing and can be tailored for methanol or FT synthesis, as shown in Extended Data Figs. 2 and 3, respectively, without the need of additional steps for correcting composition and/or separating undesired by-products. Specifically, the need for the endothermic reverse water-gas shift (RWGS) step is eliminated. In this study, the GTL unit was applied for processing solar syngas to methanol. FT synthesis of kerosene was performed with solar syngas obtained in two separate experimental setups using the same solar reactor design: with a 4-$kW_{thermal}$ solar reactor prototype operated in a high-flux solar simulator[30] and with a scaled-up 50-$kW_{thermal}$ solar reactor operated in a solar tower[31,32]. Obviously, there is no need for removal of any impurities (e.g. sulfur compounds, salts, heavy metals), as it is the case for hydrocarbons derived from petroleum. Moreover, the combustion of FT-based jet fuel, which is aromatic- and sulfur-free and is certified as aviation turbine fuel after the standard specification ASTM 7566, showed dramatic reductions in soot emissions compared to fossil-based jet fuel[33].

Discussion

Stable and successful outdoor operation of the overall system under intermittent solar irradiation convincingly demonstrates the technical viability of the thermochemical process chain for converting sunlight and ambient air to drop-in fuels. But bringing such solar fuels to the market will require substantial process optimization and upscaling, and this should be supported by policy schemes that enable market introduction at commercial scale.

A multitude of solar dishes or a heliostat field focusing on a solar tower can be used for scaling up and concentrating the DNI to the solar flux concentration required (C > 2000 suns)[8]. To appreciate the scaling needed, a commercial-scale solar fuel plant could use for example 10 heliostat fields, each collecting 100 $MW_{thermal}$ of solar radiative power, to produce 95,000 liters kerosene a day (assuming an overall system efficiency η_{system} of 10%), enough to fuel an Airbus A350 carrying 325 passengers for a London-New York roundtrip flight. The current solar fuel system uses a 5-$kW_{thermal}$ solar reactor, and while a 10x scale of the solar reactor has already been tested in a small solar tower[31,32], an additional 20x scale is still required for a 1-$MW_{thermal}$ solar reactor module, whose front quartz window is the limiting element. The commercial-size solar tower foresees an array of solar reactor modules, each attached to hexagon-shaped secondary concentrators in a honeycomb arrangement[25]. Further assembling the array of solar reactor modules in at

least two clusters and focusing the heliostat field alternately onto each cluster would enable the continuous operation of both redox steps of the cycle. This re-focusing of the heliostat field should be feasible with current hardware/software control but its dynamics still need to be proven in the field.

The layout of a commercial-scale solar fuel plant with ten solar towers, each for 100 $MW_{thermal}$, is depicted in Extended Data Fig. 6. Its complexity would be comparable to that of a concentrated solar power (CSP) plant, for which incremental scaling has taken place. The estimated land footprint would be 3.8 km^2, of which 80% is covered by the ten heliostat fields. The layout of each heliostat field (active reflecting surface = 0.1 km^2; heliostat aperture = 6.7 m^2) was generated using a ray-tracing code[34] for +31° latitude. The required frontal area of the DAC subsystem, based on a modular design using the technology applied in the present solar fuel system, would be about 4500 m^2 for capturing approximately 100,000 tons CO_2/year needed for the process, and the land area covered would represent less than 1% of the total land footprint. Thus, the DAC modules can be arranged in a single row to avoid drawing CO_2-depleted air. Assuming η_{system} = 10%, such a solar fuel plant would produce about 34 million liters kerosene/year. To put this in context, 2019 global aviation kerosene consumption was 414 billion liters[3]; the total land footprint of all solar plants required to fully satisfy global demand would be about 45,000 km^2, equivalent to 0.5% of the area of the Sahara Desert.

An important indicator of the economic feasibility of the solar fuel system is its overall energy conversion efficiency, i.e. the system efficiency η_{system} − defined as the ratio of the heating value of the liquid fuel produced to the total energy input to the system −, which in turn results from multiplying the energy efficiencies of each of the three units of the process chain: $\eta_{system} = \eta_{DAC} \cdot \eta_{solar\ redox\ unit} \cdot \eta_{GTL}$ (detailed formulation in Methods). In the present demonstration, we undertook no attempt to optimize the units for maximum η_{system}. With thermal management, the DAC unit can predominantly be driven by waste heat at below 100°C, available for example from the solar redox unit, while the GTL unit can be operated auto-thermally, thus minimizing the energy penalties upstream and downstream of the solar redox unit. Electricity would still be needed to operate the pumps in the DAC unit (desorption step at below 0.1 bar), the solar redox unit (reduction step at below 0.05 bar), and GTL unit (synthesis step at above 20 bar). However, the energy efficiency of the solar redox unit $\eta_{solar\ redox\ unit}$ dominates. It results from multiplying the optical efficiency $\eta_{optical}$ of the solar concentrator (defined as the ratio of the solar radiative energy input to the solar reactor, Q_{solar}, to the DNI incident on the solar primary concentrator) and the solar-to-syngas energy efficiency $\eta_{solar\text{-}to\text{-}syngas}$ of the solar reactor (defined as the ratio of the heating value of the syngas produced to the sum of Q_{solar} and any other parasitic energy inputs such as those associated with vacuum pumping and/or inert gas consumption). Based on the measured performance of the present solar redox unit and accounting for the energy penalties associated with vacuum pumping and inert gas recycling, $\eta_{optical}$ = 59.6%[30] and $\eta_{solar\text{-}to\text{-}syngas}$ = 1.9 – 3.8%, yielding $\eta_{solar\ redox\ unit}$ = 1.1 – 2.3%. Furthermore, we assume $\eta_{DAC} \approx 0.90$ (accounting for the energy penalty of vacuum pumping, but assuming waste heat thermal management) and $\eta_{GTL} \approx 0.75$ (using the measured syngas-to-methanol conversion and accounting for the energy penalty of gas compression, but assuming auto-thermal synthesis). Thus, the present non-optimized solar fuel system of Fig. 1 has currently $\eta_{system} \approx 0.8\%$. Several measures can be readily implemented to boost η_{system}. For example, by minimizing surface and tracking errors, $\eta_{optical}$ can be increased to 82%[27]. Notably, the optical components for concentrating the DNI, e.g. solar dishes and heliostat fields, are already established for CSP plants, though for lower values of solar flux concentration, but there are substantial technological spillovers from solar thermal electricity to solar thermochemical fuels. On the other hand, the low value obtained for $\eta_{solar\text{-}to\text{-}syngas}$ is mainly due to the sensible heat rejected during the temperature-swing cycling, which accounted for more than 60% of Q_{solar}. This fraction can be partially recovered via thermocline heat storage, as demonstrated with a packed bed of Al_2O_3 spheres that recovered half of it for

a temperature swing between 1400 and 900 °C[35]. Recovering most of it would raise $\eta_{\text{solar-to-syngas}}$ to over 20%[22,36,37]. Furthermore, there is room for optimization of the ceria structure, for example by means of 3D-printed hierarchically ordered structures with a porosity gradient for improved volumetric absorption[38]. Thus, by means of optimized porous structures, superior redox materials, improved concentrating optics, heat recovery between the redox steps, and thermal management to enable thermo-neutral operation of the DAC and GTL units, η_{system} has the potential of exceeding 13% (Methods) and possibly surpassing that of the PV-electrolysis based pathway[15,39,40]. This is because the later requires the production of substantial excess H_2 by water electrolysis using solar electricity, which is subsequently consumed via the endothermic RWGS reaction to obtain syngas suitable for the GTL step. In contrast, the present thermochemical approach bypasses the solar electricity generation, the electrolysis, and the RWGS steps, and directly produces solar syngas of desired composition, i.e. three steps are replaced by one.

Techno-economic analyses of the complete process chain analogous to the pathway demonstrated in this study[40-42] estimated a jet fuel cost in the range 1.2 – 2 €/liter. These cost values are predominantly sensitive to the energy efficiencies (assumed η_{system} = 4.4 – 11.7%), the CO_2 costs (assumed 100 €/ton CO_2, consistent with the long-term cost target[43]), and the manufacturing costs of the heliostat field, which typically represent half of the total investments costs of the solar fuel system (assumed 100 €/m^2; currently in the 100-150 €/m^2 range; DOE Sunshot's target is 75 USD/m^2). This also explains the strong dependency of the fuel cost on the solar reactor performance because the higher $\eta_{\text{solar-to-syngas}}$ the smaller becomes the heliostat field for a given Q_{solar}, and consequently the lower the investments costs of the solar concentrating infrastructure. The auxiliary components at the interface between the three main processing subsystems, such as gas pipelines, compressors, storage tanks, and other balance-of-plant components, are embedded within the given range of cost values of the fuel. The compression and storage of CO_2 and syngas in the buffer tanks represent 9.5% of the investment costs[42], but can have a significant effect on η_{system} and ultimately on the annual O&M costs because of their electricity consumption; optimized integration to minimize storage size and learning-by-doing are warranted as the system undergoes upscaling. In particular, substantial R&D and implementation of heat recovery in the solar reactor[35-37] are needed to achieve the 20% value of $\eta_{\text{solar-to-syngas}}$ assumed in the economic analyses. As expected, solar thermochemical fuels are most competitively produced in desert regions with high DNI (> 2500 kWh/m^2 per year)[41,42]. In contrast to biofuels, which are limited by resource provision, global jet fuel demand can be met by utilizing less than 1% of the worldwide arid land[41], which does not compete with food or fodder production. Furthermore, the solar fuel production chain's life cycle assessment indicates 80% avoidance of greenhouse gas emission with respect to conventional fossil jet fuel, with emissions in the range 0.1-0.6 $kg_{\text{CO2-equivalent}}$ per liter jet fuel and approaching zero when construction materials (e.g. steel, glass) are manufactured using renewable energy[42], as the amount of CO_2 emitted during jet fuel combustion equals that captured from the air during its production.

Given their high initial investment cost[42], solar thermochemical fuels require policy support to see widespread deployment, leading to concomitant cost reductions initially through scaling effects and process optimization, and then through mass production of key components and learning-by-doing. Regulatory frameworks progress over time to match three phases: initial R&D and technology demonstration, market creation and system development, and market competitiveness[44-46]. Because CORSIA (Carbon Offsetting and Reduction Scheme for International Aviation) and the EU Emission Trading System aim to reduce CO_2 emissions with carbon-pricing that is too low to support market demand for solar fuels, we propose an aviation sector support scheme that would create a near-term market for the first generation of commercial solar fuel plants. As with the policy framework recently proposed by the European Commission, this would take the form of a jet fuel quota scheme, mandating aviation fuel retailers or airlines to provide proof that a certain proportion of their fuel comes from solar fuel sources (Methods). The initial costs of such a policy

would be small enough to be politically practicable because the initial quota would be very low relative to overall jet fuel demand. For example, as described above, a commercial-scale solar fuel plant with ten solar towers, each for 100 $MW_{thermal}$ with η_{system} = 10%, would produce less than 0.01% of global jet fuel consumption. Even with an initial cost exceeding 10 USD per liter solar jet fuel (compared to less than 1 USD per conventional jet fuel) for the first ten of such solar fuel plants built, the financial impact of supplying 0.1% of the market would be small while still enabling the deployment of production facilities. This would start solar fuels' journey down the learning curve, which is the main aim of the policy. Technological learning at the same pace as for CSP – approximately 60% generation cost reduction in 15 years[47,48] – seems feasible for solar thermochemical fuels as well. Importantly, solar drop-in fuels can utilize existing storage, distribution, and utilization infrastructure and thus require no new technologies beyond the production chain. The demonstration that carbon-neutral hydrocarbon fuels can be produced using sunlight and air thus represents an important milestone that, with appropriate policy support, could initiate developments essential for the long-term decarbonization of the aviation sector.

Methods

Solar redox unit − Photographs of the solar redox unit, realized on the roof of the ETH's Machine Laboratory Building in Zurich, are shown in Extended Data Fig. 1. The optical design and characterization of the solar concentrator, comprising a primary sun-tracking solar paraboloidal dish coupled to a secondary planar rotating reflector, is found in Ref. 27.

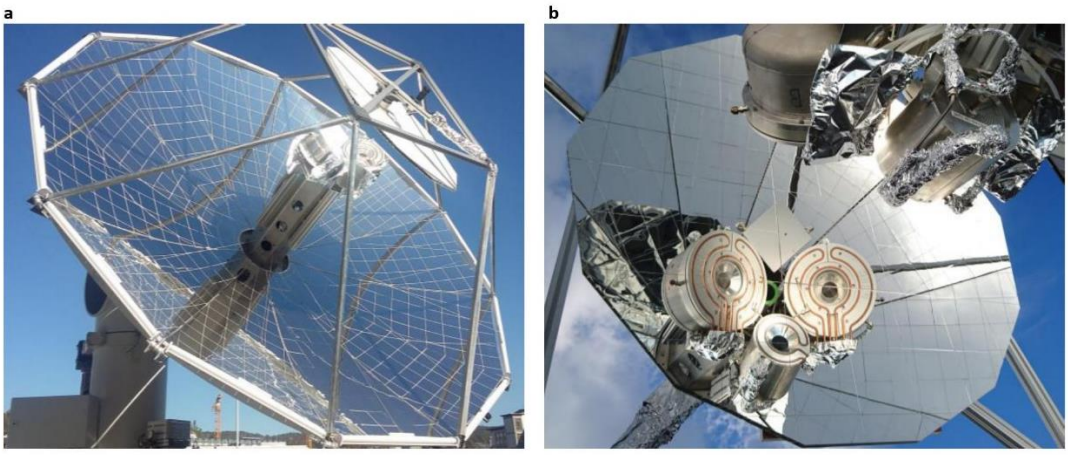

Extended Data Figure 1. Photographs of the solar fuel system at ETH Zurich. a) The solar redox unit, comprising the primary sun-tracking solar paraboloidal concentrator coupled to a secondary planar rotating reflector, and the two solar reactors at the foci. b) The two solar reactors, water-cooled calorimeter, and Lambertian target for solar radiative power measurements (seen via the secondary reflector).

Measurement instrumentation − Temperatures were measured using B-type and K-type thermocouples. Gas flow rates were regulated using Bronkhorst electronic mass flow controllers. Pressures were measured using Thermovac TTR 101N pressure sensors. A multistage roots dry vacuum pump (Adixen ACP 28CV) in combination with multiple valves (Pfeiffer Vacuum AVC 025 PA) was used to evacuate the reactors during reduction. Product gas composition was analyzed on-line downstream of the solar redox unit by gas chromatography (Agilent Technologies) and Siemens Ultramat-23 and Calomat-6 gas analysis units

(electrochemical sensors for O_2, IR detectors for CO and CO_2, thermal conductivity based detectors for H_2). The syngas was compressed using the two stage Compressor Station ILS 331. The packed-bed reactor of the GTL synthesis unit was a Microactivity Effi (PID Eng&Tech). The hemispherical spectral reflectivities of the primary concentrator and secondary reflector were measured by a spectroscopic goniometry setup using an integrating sphere (Labsphere RT-060-SF)[27]. The direct normal irradiation (DNI) was measured with a sun-tracking pyrheliometer (EKO Instruments MS-56). The solar radiative power delivered by the solar concentrating system was measured using a water-cooled calorimeter made of a selectively coated Cu-coiled cavity with the same front containing the 30 mm-radius aperture as the solar reactors. The solar flux distribution was measured with a calibrated CCD camera (Basler scA1400-17gm, manual zoom lens RICOH FL-CC6Z1218-VG, neutral density filters ND 4.8) focused on a Lambertian (diffusely-reflecting) target and verified with the water-cooled calorimeter. Both the Lambertian target and the water-cooled calorimeter were mounted at the focal plane alongside the two solar reactors (Extended Data Fig. 1b). The entire solar redox unit is controlled by a LabView program for performing fully automated consecutive redox cycles over the whole day.

Energy efficiency − The theoretical maximum solar-to-work efficiency of a thermochemical fuel production process (based on the maximum possible amount of work that may be extracted from the fuels as given by the Gibbs free energy change of their oxidation) for a blackbody solar cavity-receiver operating at an upper temperature T_H is given by[8]:

$$\eta_{\text{solar-to-work}} = \left(1 - \frac{\sigma T_H^4}{I_{DNI} \cdot C}\right)\left(1 - \frac{T_L}{T_H}\right) \quad (4)$$

where I_{DNI} denotes the DNI, C the solar concentration ratio (i.e. the solar flux intensity normalized to the DNI), T_H and T_L are the upper and lower operating temperatures of the equivalent Carnot heat engine, and σ is the Stefan-Boltzmann constant ($5.67 \cdot 10^{-8}$ $Wm^{-2}K^{-4}$). For example, assuming I_{DNI} = 1 kW/m^2 as typical for clear skies, C = 2700 suns as attainable with solar concentrating systems such as the one presented in this study, T_H = 1723 K as the upper temperature of the thermochemical process demonstrated in this study, and T_L = 300 K for rejected heat, the theoretical maximum $\eta_{\text{solar-to-work}}$ = 67.3%. This value points out to the high potential of the solar thermochemical pathway to become energy efficient and, consequently, cost effective.

System efficiency – As aforementioned, the overall energy conversion efficiency of the solar fuel system, i.e. the system efficiency η_{system}, is defined as the ratio of the heating value of the liquid fuel produced to the total energy input to the system, which in turn results from multiplying the energy efficiencies of each of the three units of the process chain:

$$\eta_{\text{system}} = \eta_{\text{DAC}} \cdot \eta_{\text{solar redox unit}} \cdot \eta_{\text{GTL}} \quad (5)$$

where

$$\eta_{\text{solar redox unit}} = \eta_{\text{optical}} \cdot \eta_{\text{solar-to-syngas}}. \quad (6)$$

The optical efficiency η_{optical} is defined as the ratio of the solar radiative energy input to the solar reactor, Q_{solar}, to the DNI incident on the solar primary concentrator. The solar-to-syngas energy efficiency $\eta_{\text{solar-to-syngas}}$ is defined as the ratio of the heating value of the syngas produced to the sum of Q_{solar} and any other parasitic energy inputs such as those associated with vacuum pumping and/or inert gas consumption during the reduction step:

$$\eta_{\text{solar-to-syngas}} = \frac{Q_{\text{fuel}}}{Q_{\text{input}}} = \frac{Q_{\text{fuel}}}{Q_{\text{solar}} + Q_{\text{pump}} + Q_{\text{inert}}} \quad (7)$$

Q_{fuel} is the heating value of the fuel (CO and H_2) produced over a cycle, given by:

$$Q_{\text{fuel}} = \sum_{\text{fuel: } H_2,CO} \Delta H_{\text{fuel}} \int r_{\text{fuel}} dt \quad (8)$$

where ΔH_{fuel} is the molar enthalpy change of fuel oxidation (e.g. ΔH_{CO} =283 kJ/mol, ΔH_{H_2} = 286 kJ/mol) and $\int r_{\text{fuel}} dt$ is the measured molar rate of the fuel produced integrated over the duration of the oxidation step. Q_{solar} is the total solar energy input integrated over the duration of the reduction step:

$$Q_{\text{solar}} = \int P_{\text{solar}} dt \quad (9)$$

where P_{solar} is the measured solar radiative power input through the solar reactor's aperture, accounting for the total transmittance of the quartz window (measured value 0.932)[49]. Q_{pump} and Q_{inert} are the thermal energy penalties associated with vacuum pumping and inert gas consumption during the reduction step. All work terms are converted to an equivalent heat by dividing by a heat-to-work efficiency $\eta_{\text{heat-to-work}}$ (assumed 0.4). In this way, the entire thermochemical process chain is driven using solar heat alone. Q_{pump} is calculated as the thermodynamic minimum pumping work divided by the product of two efficiencies, namely the heat-to-work efficiency $\eta_{\text{heat-to-work}}$ and the vacuum pump efficiency η_{pump}, according to:

$$Q_{\text{pump}} = \frac{1}{\eta_{\text{heat-to-work}} \cdot \eta_{\text{pump}}} \int \dot{n}(t) \cdot R \cdot T \cdot \ln\left(\frac{p_{\text{atmospheric}}}{p_{\text{cavity}}(t)}\right) dt \quad (10)$$

where $\dot{n}$(t) is the sum of the measured molar flow rates of Ar injected and O_2 released by ceria during the reduction step, p_{cavity} is the measured total pressure inside the cavity and $p_{\text{atmospheric}}$ is the atmospheric pressure. The pump efficiency for a multi-stage industrial arrangement is given by:

$$\eta_{\text{pump}} = 0.07 \cdot \log\left(\frac{p_{\text{cavity}}}{p_{\text{atmospheric}}}\right) + 0.4 \quad (11)$$

Note that $\eta_{\text{solar-to-syngas}}$ is weakly depended on η_{pump} because $Q_{\text{solar}} >> Q_{\text{pump}}$ at the moderate vacuum pressure levels applied during reduction in the range 10-1000 mbar. The thermal energy required for inert gas separation is given by:

$$Q_{\text{inert}} = \frac{1}{\eta_{\text{heat-to-work}}} E_{\text{inert}} \int r_{\text{inert}} dt \quad (12)$$

where r_{inert} is the measured Ar flow rate and E_{inert} is the work required for inert gas separation, assumed 20 kJ per mole[50]. Because of the relatively low mass flow rate of Ar used (typically 0.5 L min^{-1} for the present solar fuel system), Q_{inert} is less than 5% of Q_{solar}, but even this penalty can be eliminated by replacing Ar with ambient air during the reduction step as proven experimentally[25]. Furthermore, when targeting syngas for FT synthesis, CO_2 is injected after the reduction step for re-pressurizing, avoiding completely the use of inert gas.

Based on the measured performance of the present solar redox unit, $\eta_{\text{solar-to-syngas}}$ = 1.9 – 3.8%. To date, the maximum experimentally obtained $\eta_{\text{solar-to-syngas}}$ is 5.25% with a 4-kW_{thermal} solar reactor[25] and 5.6% with a 50-kW_{thermal} solar reactor[31], both solar reactors performing the CO_2 splitting redox cycle without any heat recovery. A recent experimental study reports a value of 3.17% for an efficiency defined as the ratio of the caloric value of the fuel produced over a cycle to the energy required to heat ceria and drive the endothermic reaction[51], but not accounting for the total solar energy input Q_{solar} nor the energy penalties Q_{pump} and Q_{inert}.

Energy requirements of the DAC unit – The calculated specific energy requirements are 13 kJ/mol_{CO2} of mechanical work (vacuum pump operated at 0.05 bar desorption pressure/1 bar exit pressure; 0.7 efficiency of isothermal compression), and 493-640 kJ/mol_{CO2} of heat at 95°C. These energy values were obtained for amine-functionalized nanofibrillated cellulose sorbent with a measured specific CO_2 capacity in the range 0.32-0.65 mmol/g, a specific H_2O capacity in the range 0.87-4.76 mmol/g, and an air relative humidity in the range 20-80%[10]. For a targeted sorbent's specific CO_2 capacity of 2 mmol/g, the heat requirement would be reduced to 272-530 kJ/mol_{CO2}, depending strongly on the amount of co-adsorbed water. Obviously, higher relative humidity results in more water adsorbed and, consequently, higher thermal energy requirements during the desorption step.

Efficiency potential – η_{system} is estimated for a commercial-scale solar fuel plant with 10 solar towers, each for 100 $MW_{thermal}$ (see layout depicted in Extended Data Fig. 6). Work inputs for gas compression (isothermal; 0.7 efficiency) are converted to equivalent thermal energy penalties by diving by $\eta_{heat\text{-}to\text{-}work}$ (assumed 0.4). With thermal management of heat sources and sinks, the thermal energy requirements of the DAC subsystem can be provided by waste heat available from the solar redox or the GTL subsystems. The equivalent thermal energy penalty for CO_2 vacuum pumping and compression to 10 bars represents less than 10% of Q_{solar}; thus $\eta_{DAC} \approx 0.90$. With improved concentrating optics, optimized porous structure[38], superior redox materials, and heat recovery using thermocline-based heat storage[35], $\eta_{solar\ redox\ unit} > 0.2$. The GTL unit can be operated auto-thermally (e.g. syngas-to-methanol is exothermic by ΔH = -90 kJ/mol CH_3OH). Assuming 90% mass conversion[42] and accounting for the equivalent thermal energy penalty for syngas compression to 60 bars (< 10% of Q_{solar}), $\eta_{GTL} \approx 0.75$. Finally, by applying Eq. 5, η_{system} has the potential of exceeding 13%.

Solar syngas production for methanol or FT synthesis – Extended Data Figs. 2 and 3 show two cases of an exemplary redox cycle for co-splitting H_2O and CO_2 and producing solar syngas with compositions suitable for either methanol synthesis (Extended Data Fig. 2) or FT synthesis (Extended Data Fig. 3). Results are summarized in the Extended Data Table 1. The temporal variation of the nominal cavity temperature, total pressure, and outlet gas flow rates during a single redox cycle are plotted for both cases in Extended Data Figs. 2a and 3a. The solar radiative power input is maintained relatively constant on a clear sunny day at P_{solar} = 5.1 $kW_{thermal}$ and 4.1 $kW_{thermal}$ for the runs of Extended Data Fig. 2a and 3a, respectively. In both cases, the reduction step proceeds under analogous operational conditions: the solar reactor is first heated with P_{solar} to the desired reduction-end temperature $T_{reduction\text{-}end}$ = 1450°C under vacuum pressure below 50 mbar. Once a nominal cavity temperature of $T_{reduction\text{-}end}$ is reached, the solar input is diverted by rotating the secondary reflector. Subsequently, the reaction chamber is re-pressurized to 1 bar by injecting either Ar for the case of syngas for methanol synthesis (Extended Data Fig. 2a) or CO_2 for the case of syngas for FT synthesis (Extended Data Fig. 3a). Passive cooling of the solar reactor induces a temperature decrease down to the oxidation-start temperature, $T_{oxidation\text{-}start}$ = 900°C and 800°C for the two cases, respectively. At that point, H_2O and CO_2 from the buffer tanks are co-injected into the solar reactor with molar ratios H_2O:CO_2 = 12.5 and 24.9, to produce desired compositions of syngas for either methanol or FT synthesis, respectively. The temporal variation of the cumulative species concentrations and yields of solar syngas collected during the oxidation step for either methanol or FT synthesis are plotted in Extended Data Fig. 2b and Extended Data Fig. 3b, respectively. Time 0 denotes the start of the oxidation when the nominal reactor temperature reaches $T_{oxidation\text{-}start}$. Note the absence of Ar in the syngas for FT synthesis because CO_2 was used instead to re-pressurize the solar reactor after the reduction step. Apart from selecting the $T_{oxidation\text{-}start}$ and the inlet flow rates of H_2O and CO_2, the composition of the syngas can be adjusted by choosing adequate start and end times of the syngas collection. For example, immediately after the start of the oxidation step, the syngas contains undesired high content of Ar (Extended Data Fig. 2b) or CO_2 (Extended Data Fig. 3b), but we can improve the syngas quality by simply delaying the start of

the syngas collection. On the other hand, the end of the syngas collection can be determined once the desired molar ratio (H_2:CO_x for methanol synthesis or H_2:CO for FT synthesis) of the collected syngas is achieved. In fact, the desired molar ratio H_2:CO_x of syngas suitable for methanol synthesis lies between 2 and 3 (depending on the CO:CO_2 molar ratio and on the catalyst used) and can be accomplished by collecting the syngas over the period between 2 to 10 minutes in Extended Data Fig. 2b, yielding H_2:CO_x = 2.58. The desired molar ratio H_2:CO of syngas suitable for FT synthesis is about 2 and can be accomplished by collecting the syngas over the period between 0 to 4.25 minutes in Extended Data Fig. 3b, yielding H_2:CO = 2. Evidently, there is a trade-off between syngas quality and syngas quantity.

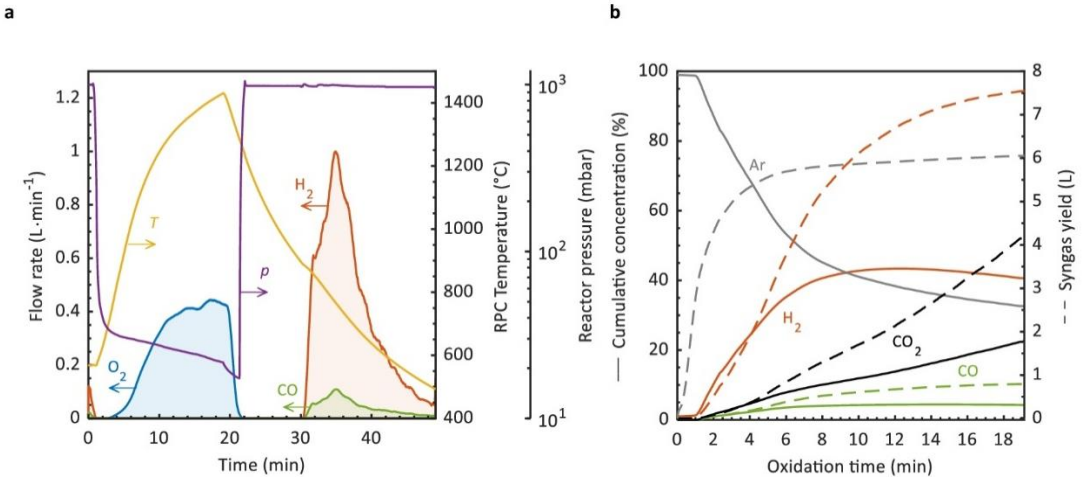

Extended Data Figure 2. Representative solar redox cycle producing syngas with composition suitable for methanol synthesis. a) Temporal variation of the nominal cavity temperature, total pressure, and outlet gas flow rates during a single redox cycle. b) Temporal variation of the cumulative species concentration and yield of solar syngas collected during the oxidation step. Operation conditions – During the reduction step: Q_{solar} = 5.1 kW, inlet flow 0.5 L/min Ar, $T_{reduction\text{-}end}$ = 1450°C, total pressure ≤ 25 mbar. During the oxidation step: Q_{solar} = 0 kW, inlet flows 0.4 L/min CO_2 + 9.8 g/min H_2O, $T_{oxidation\text{-}start}$ = 900°C, total pressure = 1 bar.

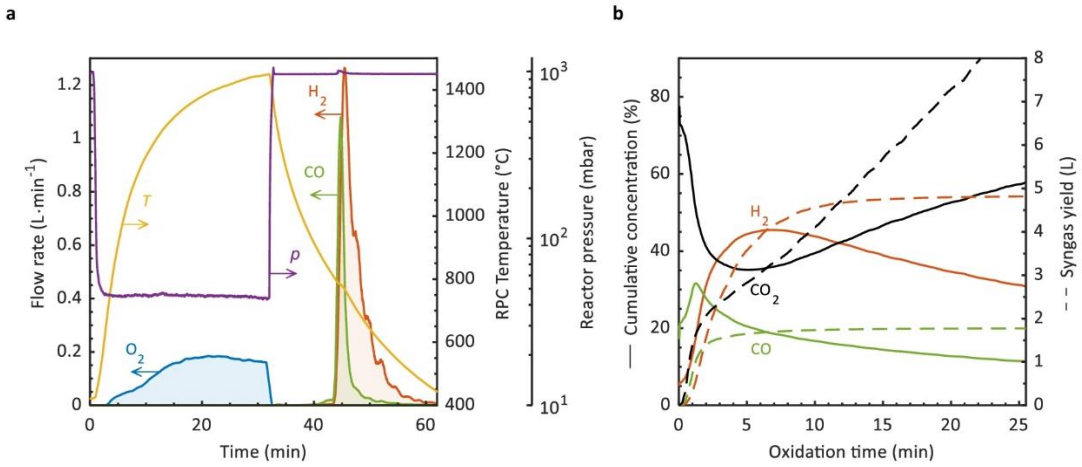

Extended Data Figure 3. Representative solar redox cycle producing syngas with composition suitable for FT synthesis. a) Temporal variation of the nominal cavity temperature, total pressure, and outlet gas flow rates during a single redox cycle. b) Temporal variation of the cumulative species concentration and yield of solar syngas collected during the oxidation step. Operation conditions – During the reduction step: Q_{solar} = 4.1 kW, inlet flow 0.5 L/min Ar, $T_{reduction\text{-}end}$ = 1450°C, total pressure ≤ 50 mbar. During the oxidation step: Q_{solar} = 0 kW, inlet flows 0.2 L/min CO_2 + 9.8 g/min H_2O, $T_{oxidation\text{-}start}$ = 800°C, total pressure = 1 bar.

Preprint version of the article: Schäppi, R., Rutz, D., Dähler, F., Muroyama, A., Haueter, P., Lilliestam, J., Patt, A., Furler, P., Steinfeld, A. (2022): Drop-in fuels from sunlight and air, in Nature 601, pp. 63-68. https://doi.org/10.1038/s41586-021-04174-y.

Extended Data Table 1: Summary of syngas quality for the experimental runs of Extended Data Fig. 2 for methanol synthesis and Extended Data Fig. 3 for FT synthesis.

	Syngas for methanol synthesis		*Syngas for Fischer-Tropsch synthesis*	
	Extended Data Figure 4b		Extended Data Figure 5b	
Collection times	0 - 20 min	2 - 10 min	0 - 25 min	0 - 4.25 min
Amount (L/cycle)	18.5	9.4	15.6	7.52
Composition	40.7% H_2 4.3% CO 22.4% CO_2 32.6% Ar	59.9% H_2 6.0% CO 17.2% CO_2 16.9% Ar	31.0% H_2 11.4% CO 57.6% CO_2	43.1% H_2 21.5% CO 35.4% CO_2
Stoichiometry	H_2:CO_x = 1.52	H_2:CO_x = 2.58	H_2:CO = 2.72	H_2:CO = 2
CO_2 conversion	16.1%	25.7%	16.5%	37.9%

When generating syngas for methanol synthesis (Extended Data Fig. 2b), the full oxidation cycle over 20 min yields 18.5 L of syngas with composition 40.7% H_2, 4.3% CO, 22.4% CO_2 and 32.6% Ar. The resulting molar ratio H_2:CO_x is 1.52, which is not optimal for methanol synthesis. Besides, the CO_2 conversion – integrated over the full oxidation period – is only 16.1%. Alternatively, collecting the syngas between minutes 2 and 10 (Extended Data Fig. 2b) would yield instead only 9.4 L of syngas, i.e. only about half the amount, but with a more favorable composition of 59.9% H_2, 6.0% CO, 17.2% CO_2 and 16.9% Ar. The resulting molar ratio H_2:CO_x would be 2.58, and thus suitable for methanol synthesis. The CO_2 conversion – integrated over minutes 2 to 10 – would be now 25.7%. Furthermore, the Ar content would be cut in half, reducing the energy penalty of carrying an inert gas downstream. Nevertheless, a scale-up of the process would require either Ar separation and recycling or ways to avoid the use of inert gas for re-pressurizing during the switch from the reduction step to the oxidation step. In terms of energy efficiency, $\eta_{\text{solar-to-syngas}}$ is affected in both directions because, although the amount of syngas is reduced, the duration of both redox steps can be made shorter and Q_{solar} is therefore smaller (see Eqs. 6-8).

When generating syngas for FT synthesis (Extended Data Fig. 3b), the full oxidation after 25 min yields 15.6 L of syngas with composition 31.0% H_2, 11.4% CO and 57.6% CO_2 with a molar ratio H_2:CO = 2.72, which is not optimal for FT synthesis. The CO_2 conversion – integrated over the full oxidation period – is only 16.5%. Collecting the syngas between minutes 0 and 4.25 of the oxidation cycle (Extended Data Fig. 3b) would yield only 7.52 L of syngas, i.e. only about half the amount, but with a more favorable composition of 43.1% H_2, 21.5% CO and 35.4% CO_2. The resulting molar ratio would be exactly H_2:CO = 2, and thus suitable for FT synthesis. The CO_2 conversion – integrated over minutes 0 to 4.25 – would now be 37.9%. Note that the operational conditions during the oxidation step (CO_2/H_2O mass flow rates and $T_{\text{oxidation-start}}$) are different for the run targeting syngas for methanol synthesis and the one targeting syngas for FT synthesis. In general, the duration of the oxidation becomes shorter with higher mass flow rates and the syngas yield increases with $T_{\text{oxidation-start}}$ because of faster reaction rates. Note further that, in contrast to the runs of Extended Data Figs. 2 and 3, the oxidation steps in the consecutive cycles of Fig. 2 were not executed until completion but they were simply terminated prematurely by the end of syngas collection to avoid additional passive cooling of the cavity and enable shorter cycle durations.

In both redox cycles for Extended Data Figs. 2 and 3, the oxygen mass balance can be closed within the error bars of the measurement devices (electronic mass flow controllers and the electrochemical and IR gas analysis), confirming total selectivity for the conversion of H_2O to H_2 and of CO_2 to CO, with net reactions $H_2O = H_2 + ½O_2$ and $CO_2 = CO + ½O_2$. Total selectivity was obtained in all cycles performed with the solar reactor, i.e. only the reduction (Eq. 1) and oxidation (Eq. 2/3) reactions occur.

Long-term consecutive solar redox cycling for methanol production – Extended Data Fig. 4 shows the syngas composition and yield for each of the 152 consecutive solar redox cycles. In contrast to the day run of Fig. 2, which was performed on a clear day with constant DNI and yielded steady syngas composition from cycle to cycle, this long-term run was performed over several days and yielded significant variations in the syngas composition from cycle to cycle, primarily due to the unstable DNI, which in turn affected the solar radiative power input, the heating rates and temperature distributions, and the reduction and oxidation rates and extents. As the run progressed, the H_2O and CO_2 mass flow rates were adjusted to ensure syngas collection with a cumulative molar ratio H_2:CO_x in the range 2-3. The reactants' flow rates during the oxidation step were 0.4 L/min CO_2 and 10 g/min H_2O for cycles 1 to 37, and 0.3 L/min CO_2 and 10 g/min H_2O for cycles 38 to 152. During the first 17 cycles, a molar ratio H_2:CO_x = 2 was targeted. From cycle 18 onwards, a cumulative molar ratio H_2:CO_x = 2.5 over the entire 152 cycles was targeted. Extended Data Fig. 5 shows the cyclic variation and cumulative molar ratio H_2:CO_x for the 152 redox cycles of Extended Data Fig. 4. The total yield was 1069.7 L of syngas with composition 58.4% H_2, 5% CO, 18.6% CO_2 and 18% Ar (after condensation of unreacted water). Thus, the cumulative molar ratio obtained was H_2:CO_x = 2.48. This solar syngas was further processed to methanol in the GTL unit.

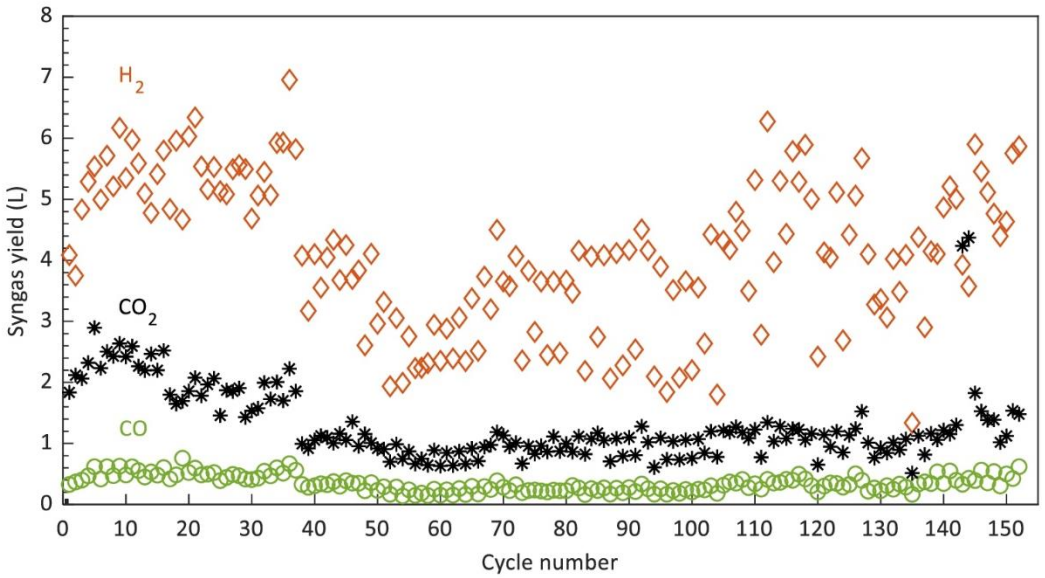

Extended Data Figure 4. Syngas yield (H_2 in orange, CO in green, CO_2 in black) for each of the 152 consecutive solar redox cycles. L denotes standard liters.

Preprint version of the article: Schäppi, R., Rutz, D., Dähler, F., Muroyama, A., Haueter, P., Lilliestam, J., Patt, A., Furler, P., Steinfeld, A. (2022): Drop-in fuels from sunlight and air, in Nature 601, pp. 63-68. https://doi.org/10.1038/s41586-021-04174-y.

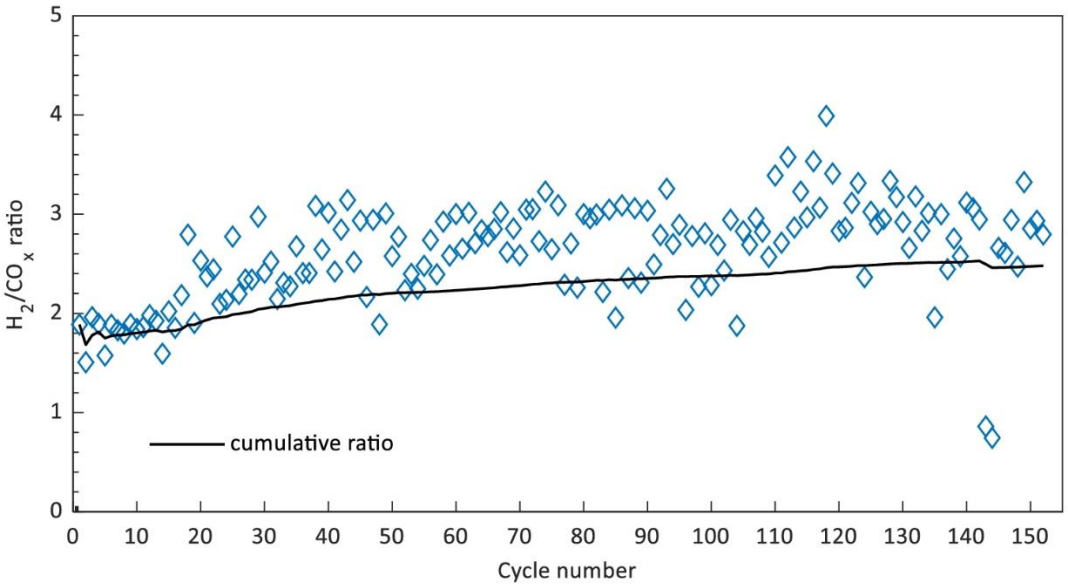

Extended Data Figure 5. Cyclic variation (blue data points) and cumulative (black curve) molar ratio H_2:CO_x for the 152 consecutive redox cycles of Extended Data Fig. 4.

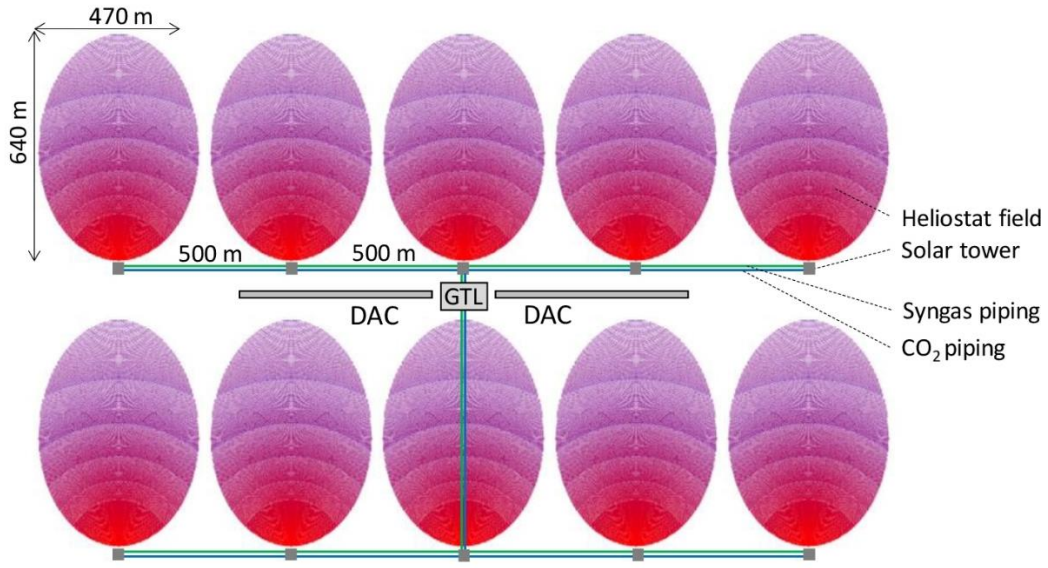

Extended Data Figure 6. Simplified layout of a commercial-scale solar fuel plant with ten solar towers, each for 100 $MW_{thermal}$. DAC: Direct Air Capture; GTL: Gas-to-Liquid.

Integration of the solar fuel system − The CO_2 and water streams exiting the DAC unit are stored in a 750 l steel buffer tank and in a plastic buffer tank, respectively, so they can be delivered to the solar redox unit according to demand. If the CO_2 tank reaches 12 bars, usually after 48 hours operation, the DAC unit is automatically idled until demand is present. The full CO_2 buffer tank can typically support between 3 to 18 days of operation of the solar redox unit, depending on the specific fuel targeted, e.g. 3 to 5 days for CO_2 splitting only. The buffer tanks also balance the mismatch between the amount of water obtained in the DAC unit (H_2O:CO_2 ≈ 6.1-12.2, depending on the air relative humidity) and that used in the solar redox unit (H_2O:CO_2 ≈ 12.5-24.9, depending on the targeted fuel), with excess unreacted water collected downstream of the solar reactor recycled. The molar ratios H_2O:CO_2 of reactants fed to the solar redox unit were significantly higher than the stoichiometric ones (Extended Data Table 1), pointing out to the excess water fed into the solar reactor. Because CO_2 dissociation proceeds more readily than that of H_2O at equal conditions[28], a large excess of H_2O over CO_2 had to be introduced into the solar reactor to obtain the desired syngas compositions. The excess water introduces significant energy penalties associated with steam generation and heating unreacted species, although a portion of the sensible heat can be recovered. The syngas stream produced by the solar redox unit is stored in a 5-liter buffer gas cylinder at up to 250 bar for delivery to the GTL unit as per demand. Syngas storage means that the GTL unit can in principle be operated continuously round-the-clock, though intermittent daily startup-shutdown operation of the GTL unit for methanol synthesis at the lab scale is possible by purging the catalyst with H_2-free gas upon shutdown to avoid deactivation[52]. This option reduces the cost of storing syngas, but at a large scale is generally avoided due to the complications associated with operating intermittently an oversized GTL unit.

Evidently, the coupling of the intermittent solar redox process with the round-the-clock DAC and GTL processes complicates the integration of the three units because of the temporal mismatch of both mass and energy flow rates to/from each unit. Further complication arises from the different operational temperatures and pressures of each unit. In terms of the mass flows, the incorporation of buffer tanks upstream and downstream of the solar redox unit to intermediately store H_2O and CO_2 (upstream) and syngas (downstream), as applied in this solar fuel system, is technically simple and scalable, and therefore the preferred approach as compared to running the entire system only during sunshine hours with oversized (and more expensive) DAC and GTL units. The sizing of these buffer tanks for an industrial-scale plant is a function of the mass flow rates of reactants/products to/from the solar redox unit, which operates up to 10 hours/day. In terms of the energy flows, the thermal management discussed above as a measure to maximize η_{system} would be practicable by heat exchange via heat transfer fluids between the endothermic DAC process (heat sink at below 100°C) and the exothermic GTL process (heat source at above 200°C). However, heat exchange with the solar-driven process would be possible only if heat is stored temporarily, for example in thermocline heat storage tanks[35].

An alternative solar redox unit configuration, which would potentially simplify its integration, consists of replacing the solar reactor at the focus of the solar concentrator for a solar receiver that delivers high-temperature heat via a heat transfer fluid to a thermal storage tank, which in turn continuously delivers heat to a (non-solar) redox reactor. Such a reactor, or array of reactors, would operate round-the-clock similar to the power block of a CSP plant with thermal storage[8], and therefore would be simpler to integrate with the DAC and GTL units, both in terms of the mass and energy flow rates. Thermal management would be applicable by heat exchange with the redox reactor as well. Furthermore, this configuration would facilitate the operation of the oxidation step at higher, thermodynamically more favorable pressures to obtain pressurized syngas, thereby minimizing or even eliminating the compression work before the GTL.

Perhaps the most critical aspect of integration is the suitability of the gas streams exchanged between the units, namely the quality and purity of CO_2 and H_2O exiting the DAC unit and fed to the solar redox unit, and the quality and purity of the syngas exiting the solar redox unit and fed to the GTL unit. The solar fuel

system fulfilled the suitability criterion without the need for additional refinement steps, such as the energy-intensive RWGS step, and thereby reaffirmed the potential for high η_{system} (Eq. 5).

Technology deployment at scale − As is so often seen with new technologies (c.f. the improvements in efficiency and drop in cost of solar panels), deployment of solar fuels at scale can be expected to result in significant cost reductions. In part, this will be due to the economies of scale affecting both the solar fuel production units (e.g. array of solar towers) and production of necessary hardware (e.g. larger factories manufacturing critical components). In fact, scaling up has substantially reduced the cost of CSP[48,53] and the same beneficial effect will likely be seen with solar thermochemical fuels. A second benefit of technology deployment at scale is that it pushes manufacturers to engineer improved systems and operators to optimize system implementation and operation. Given the complexity of solar thermochemical fuel production that involves distinct and interlinked processes, we envisage that feedback from operation to manufacturing will be essential to learning-by-interacting within the supply chain will be essential to identify best practice and best design[54]. A further source of learning is technological spillover from other applications using the same components, prominently from CSP, DAC, and GTL applications.

Regulatory policy frameworks − We consider the policy frameworks that could be employed to incentivize growing production of solar fuels, as described in this article, to the point where they can meet full global demand by 2050. As a starting point, there are clear parallels between the current goal of accelerating a transition from fossil to solar fuels, and the goal faced twenty years ago of beginning to shift electric power from fossil-fired to solar PV generation. When countries first began to stimulate investment in PV, its cost was roughly ten times that of fossil-fired power and there was little confidence about maintaining grid stability if PV were to contribute more than 20% of demand[55]. By stimulating investment, however, the PV industry grew, and that in turn led to innovation and cost reductions[56]. Research suggests that direct government support for new technologies is often essential to enable and accelerate their becoming established in the market, which is a prerequisite for cost reductions[45]. Neo-classical economic models often assume that innovations occurred primarily in the laboratory in direct response to investments into R&D[57]. More recent studies show, however, that while R&D funding is essential during the invention stage, it plays little role in achieving cost reductions[58]. These, instead, occur as a direct result of growing commercial-scale investments in the new technologies, through the mechanisms of learning-by-doing and mass production[59]. The key to achieving cost reductions is then to stimulate investment in commercial-scale production facilities. To do so, policy makers need to overcome two main barriers: the high average cost of the new technology, and the high perceived risks associated with the new technology's performance and market viability[60]. The most successful policy instruments are those that create predictable demand at sufficiently high prices to guarantee profitability of investments into the new technologies over the amortization period, typically 20-25 years[45], minimizing the risks of stranded assets.

With these goals in mind, policy makers have employed several policy instruments to support renewable energy deployment, summarized in Extended Data Table 2. Of these, feed-in tariffs and quota systems have performed the best. Because they manage risk so well, feed-in tariffs have enabled project developers to obtain close to risk-free debt financing, which has resulted in lower costs[59]. Quota systems have also performed well, especially in regulatory environment favoring long-term power purchase agreements (PPAs), which achieve the same level of certainty as a feed-in tariff. Quota schemes in which the market sets the support level through trade of green certificates have fared much less well, mainly due to the high price and volume risks faced by investors[61,62]. The one instrument that has generally failed to stimulate new investments, and hence failed to trigger learning effects, is carbon pricing, whether in the form of a carbon tax or a carbon allowance market[61]. This is because carbon prices have generally been too low to cover the expected cost differential between renewable and fossil-fired power[62], and have failed to address the uncertainties of future power prices and of the carbon price itself[63]. The empirical literature also suggests

that when there are competing technologies at different levels of maturity, technology-neutral policies have the effect of stimulating investment – and hence learning – in the more mature technologies, even if the long-term growth prospects for the less mature technology are better[64,65].

Extended Data Table 2: Support policy instruments.

Instrument	*Mechanism*	*Examples*
Feed-in tariff	Project developers have the right to sign a long-term contract with the grid operator, to sell all power fed into the grid at a price fixed for typically 15-25 years	Germany, Spain, Italy, Switzerland, Czech Republic, China
Quota	Grid operators need to provide certificates demonstrating that a minimum share of the power they supply comes from renewable sources; price set in PPA or certificate trade	Numerous US states, United Kingdom, Netherlands
Investment subsidy	Project developers receive a one-time subsidy, covering a portion of the investment costs	United States, Switzerland
Production subsidy	Project operators receive a subsidy in addition to the market price for each unit of electricity that they sell	United States
Carbon price	Consumers of fossil fuels pay a surcharge – either as a tax or as the price of a traded permit – for each ton of carbon they emit	European Union, Sweden, Switzerland

Solar aviation fuels can in some respects be compared in their present state to solar power roughly 20-30 years ago. First, they are much more expensive than the fossil kerosene they are meant to replace. Second, it is unclear whether they will ever achieve cost parity. Third, they face competing technologies in the sustainable aviation fuels market, e.g. bio-kerosene, which is currently more mature, yet ultimately limited in the long-term scalability because of its environmental effects and limited cultivable land. Based on the experience from other renewable energy policies, it is apparent that a technology-specific direct support mechanism could be effective in stimulating investment into solar aviation fuels.

Preprint version of the article: Schäppi, R., Rutz, D., Dähler, F., Muroyama, A., Haueter, P., Lilliestam, J., Patt, A., Furler, P., Steinfeld, A. (2022): Drop-in fuels from sunlight and air, in Nature 601, pp. 63-68. https://doi.org/10.1038/s41586-021-04174-y.

References

1 Grewe, V., Gangoli Rao, A., Grönstedt, T. *et al.* Evaluating the climate impact of aviation emission scenarios towards the Paris agreement including COVID-19 effects. *Nat Commun* **12,** 3841 (2021).

2 Chen J. et al. The relationship between the development of global maritime fleets and GHG emission from shipping. *Journal of Environmental Management* **242**, 31-39 (2019).

3 International Energy Agency (2021). World demand by product groups, 2018-2019, IEA, Paris. https://www.iea.org/data-and-statistics/charts/world-demand-by-product-groups-2018-2019.

4 Schäfer, A. et al. Technological, economic and environmental prospects of all-electric aircraft. *Nature Energy* **4**, 160–166 (2019).

5 Lewis, N.S., & Nocera, D.G. Powering the planet: chemical challenges in solar energy utilization. *Proc Natl Acad Sci* **103**, 15729-15735 (2006).

6 Ozin, G.A. Throwing new light on the reduction of CO2. *Advanced Materials* **27**, 1957-1963 (2015).

7 Detz, R.J. et al. The future of solar fuels: when could they become competitive?. *Energy & Environmental Science* 11, 1653-1669 (2018).

8 Romero, M. & Steinfeld, A. Concentrating solar thermal power and thermochemical fuels. *Energy & Environmental Science* **5**, 9234-9245 (2012).

9 Zeman, F. S., & Keith, D. W. Carbon neutral hydrocarbons. *Phil. Trans. R. Soc. A* **366**, 3901-3918 (2008).

10 Wurzbacher, J. et al. Concurrent separation of CO_2 and H_2O from air by a temperature-vacuum swing adsorption/desorption cycle. *Environmental Science & Technology* **46**, 9191-9198 (2012).

11 Brady, C. et al. Integration of thermochemical water splitting with CO_2 direct air capture. *Proceedings of the National Academy of Sciences of the United States of America* **116**, 25001-25007 (2019).

12 Jia, J. et al. Solar water splitting by photovoltaic-electrolysis with a solar-to-hydrogen efficiency over 30%. *Nature Communications* **7,** 13237 (2016).

13 Chalmin, A. Direct air capture: recent developments and future plans. Geoengineering Monitor (2019).

14 Roeb, M. et al. Test operation of a 100 kW pilot plant for solar hydrogen production from water on a solar tower. *Solar Energy* **85**, 634–644 (2011).

15 Vázquez, F. V. et al. Power-to-X technology using renewable electricity and carbon dioxide from ambient air: SOLETAIR proof-of-concept and improved process concept. *Journal of CO2 Utilization* **28**, 235-246 (2018).

16 Chueh, W.C. & Haile, S.M. A thermochemical study of ceria: exploiting an old material for new modes of energy conversion and CO2 mitigation. *Philosophical Transactions of the Royal Society A: Mathematical, Physical and Engineering Sciences* **368**, 3269-3294 (2010).

17 Abanades, S. & Flamant, G. Thermochemical hydrogen production from a two-step solar-driven water-splitting cycle based on cerium oxides. *Solar Energy* **80**, 1611-1623 (2006).

18 Madhusudhan, J, et al. Reversible phase transformations in novel Ce-substituted perovskite oxide composites for solar thermochemical redox splitting of CO_2. *Advanced Energy Materials* **11**, 2003532 (2021).

19 McDaniel, A. H. et al. Sr- and Mn-doped LaAlO3-δ for solar thermochemical H2 and CO production. *Energy & Environmental Science* **6**, 2424-2428 (2013).

20 Muhich, C.L. et al. Efficient generation of H_2 by splitting water with an isothermal redox cycle. *Science* **341**, 540-542 (2013).

21 Bayon, A. et al. Operational Limits of Redox Metal Oxides Performing Thermochemical Water Splitting. Energy Technol. 2100222 (2021). DOI: 10.1002/ente.202100222

22 Ermanoski, I. et al. Efficiency maximization in solar-thermochemical fuel production: challenging the concept of isothermal water splitting. *Physical Chemistry Chemical Physics* **16**, 8418-8427 (2014).

23 Abanades S. et al., Synthesis and thermochemical redox cycling of porous ceria microspheres for renewable fuels production from solar-aided water-splitting and CO2 utilization. *Appl. Phys. Lett.* **119**, 023902 (2021).

24 Chueh, W.C. et al. High-flux solar-driven thermochemical dissociation of CO_2 and H_2O using nonstoichiometric ceria. *Science* **330**, 1797-1801 (2010).

25 Marxer, D. et al. Solar thermochemical splitting of CO_2 into separate streams of CO and O_2 with high selectivity, stability, conversion, and efficiency. *Energy & Environmental Science* **10**, 1142-1149 (2017).

26 Furler, P. et al. Thermochemical CO_2 splitting via redox cycling of ceria reticulated foam structures with dual-scale porosities. *Physical Chemistry Chemical Physics* **16**, 10503-10511 (2014).

27 Dähler, F. et al. Optical design and experimental characterization of a solar concentrating dish system for fuel production via thermochemical redox cycles. *Solar Energy* **170**, 568-575 (2018).

28 Furler, P. et al. Syngas production by simultaneous splitting of H_2O and CO_2 via ceria redox reactions in a high-temperature solar reactor. *Energy & Environmental Science* **5**, 6098-6103 (2012).

29 Schäppi, R., et al. Solar Thermochemical Splitting of CO2 in a Modular Solar Dish-Reactor System. *Proc. ISES-SWC2019 Solar World Congress*, Santiago, Chile, Nov. 4-7, 2019. doi:10.18086/swc.2019.24.08

30 Marxer, D. et al. Demonstration of the entire production chain to renewable kerosene via solar thermochemical splitting of H_2O and CO_2. *Energy Fuels* **29**, 3241-3250 (2015).

31 Zoller, S. A 50 kW solar thermochemical reactor for syngas production utilizing porous ceria structures. Diss. ETH No. 26451 (2020).

32 Romero, R. et al. Solar-Driven Thermochemical Production of Sustainable Liquid Fuels from H_2O and CO_2 in a Heliostat Field. *Proc. ISES-SWC2019 Solar World Congress*, Santiago, Chile, Nov. 4-7, 2019. doi:10.18086/swc.2019.23.02.

33 Corporan, E. et al. Emissions characteristics of a turbine engine and research combustor burning a Fischer-Tropsch jet fuel. *Energy Fuels* **21**, 2615-2626 (2007).

34 SolarPILOT software version 2015.10.5, National Renewable Energy Laboratory (NREL), https://www.nrel.gov/csp/solarpilot.html.

35 Geissbühler, L. Thermocline thermal energy storage: advances and applications to CSP, compressed air energy storage, and solar fuels. Diss. ETH No. 24555 (2017).

36 Scheffe, J.R. & Steinfeld, A. Thermodynamic Analysis of Cerium-based Oxides for Solar Thermochemical Fuel Production. *Energy Fuels* **26**, 1928-1936 (2012).

37 Lapp, J. et al. Efficiency of two-step solar thermochemical non-stoichiometric redox cycles with heat recovery. *Energy* **37**, 591-600 (2012).

38 Hoes, M. et al. Additive-manufactured ordered porous structures made of ceria for concentrating solar applications. *Energy Technology* **7**, 1900484 (2019).

39 Wim, H. & Geerlings, H. Efficient production of solar fuel using existing large scale production technologies. *Environ. Sci. Technol.* **45**, 8609–8610 (2011).

40 Kim, J. et al. Fuel production from CO_2 using solar-thermal energy: system level analysis. *Energy & Environmental Science* **5**, 8417-8429 (2012).

41 Falter, C. et al. Geographical Potential of Solar Thermochemical Jet Fuel Production. *Energies* **13**, 802 (2020).

42 Falter, C. et al. An integrated techno-economic, environmental and social assessment of the solar thermochemical fuel pathway. *Sustainable Energy & Fuels* **4**. 3992 (2020).

43 Sutherland, B.R. Pricing CO_2 Direct Air Capture. *Joule* **3**, 1571-1573 (2019).

44 Perner, J. & Bothe, D. International aspects of a power-to-X roadmap. *Frontier Economics*, 156 (2018).

45 Patt, A. & Lilliestam, J. The case against carbon prices. *Joule* **2**, 2494-2498 (2018).

46 Rosenbloom, D. et al. Why carbon pricing is not sufficient to mitigate climate change - and how "sustainability transition policy" can help. *Proceedings of the National Academy of Sciences* **117**, 8664-8668 (2020).

47 Lilliestam, J. et al. The near- to mid-term outlook for concentrating solar power: mostly cloudy, chance of sun. Energy Sources, Part B: Economics, Planning, and Policy (2020). DOI: 10.1080/15567249.2020.1773580

48 Lilliestam, J. et al. Empirically observed learning rates for concentrating solar power and their responses to regime change. *Nature Energy* **2,** 17094 (2017).

49 Villasmil, W. et al. Dynamic modeling of a solar reactor for zinc oxide thermal dissociation and experimental validation using IR thermography. *Journal of Solar Energy Engineering* **136**, 011015-1/11 (2014).

50 Haring, H. W. *Industrial Gases Processing*, Wiley-VCH, 2008.

51 Haeussler, A. et al. Solar thermochemical fuel production from H_2O and CO_2 splitting via two-step redox cycling of reticulated porous ceria structures integrated in a monolithic cavity-type reactor. *Energy* **201**, 117649 (2020).

52 Ash-Kurlander, U. et al. A. Impact of daily startup-shutdown conditions on the production of solar methanol over a commercial Cu-ZnO-Al2O3 catalyst. *Energy Technology* **4**, 565-572 (2016).

53 Mehos, M. et al. Concentrating Solar Power Best Practices Study. Golden, CO: National Renewable Energy Laboratory. NREL/TP-5500-75763 (2020). https://www.nrel.gov/docs/fy20osti/75763.pdf

54 Malhotra, A. & Schmidt, T. Accelerating Low-Carbon Innovation. Joule **4**, 2259-2267 (2020).

55 Trancik, J. Renewable energy: Back the renewables boom. *Nature* **507**, 300–302 (2014).

56 Ferioli, F. et al. Use and limitations of learning curves for energy technology policy: A component-learning hypothesis. *Energy Policy* **37**, 2525–2535 (2009).

57 Nordhaus, W. The Climate Casino. (Yale University Press, 2013).

58 Patt, A. et al. Will policies to promote energy efficiency help or hinder achieving a 1.5°C climate target? *Energy Efficiency* **12**, 551–565 (2019).

59 Nemet, G. Beyond the learning curve: factors influencing cost reductions in photovoltaics. *Energy Policy* **34**, 3218–3232 (2006).

60 Haas, R. et al. A historical review of promotion strategies for electricity from renewable energy sources in EU countries. *Renew. Sustain. Energy Rev.* **15**, 1003–1034 (2011).

61 Lilliestam, J. et al. The effect of carbon pricing on technological change for full decarbonization: a review of ex-post evidence. *Wiley Interdisciplinary Reviews – Climate Change*, 12(1): e681. doi:10.1002/wcc.681 (2021).

62 Eskeland, G. et al.. Transforming the European energy system. in *Making climate change work for us: European perspectives on adaptation and mitigation strategies* (eds. Hulme, M. & Neufeldt, H.), 165–199, Cambridge University Press (2010).

63 Kunreuther, H. et al. Integrated risk and uncertainty assessment of climate change response policies. in Climate Change 2014: Mitigation of Climate Change. Contribution of Working Group III to the Fifth Assessment Report of the Intergovernmental Panel on Climate Change 151–205, Cambridge University Press (2014).

64 Battke, B. et al. Internal or external spillovers – Which kind of knowledge is more likely to flow within or across technologies. *Res. Policy* **45**, 27–41 (2016).

65 Patt, A. Transforming energy: solving climate change with technology policy. Cambridge University Press (2015).

Data Availability Statement: The authors declare that the main data supporting the findings of this study are available within the paper and its extended data figures. Source data for Fig. 2 and Extended Data Figs. 2,3,4 and 5 are provided with the paper.

Acknowledgements – This work was funded in part by the Swiss Federal Office of Energy (Grant No. SI/501213-01), the Swiss National Science Foundation (Grant No. 200021-162435), and the European Research Council under the European Union's ERC Advanced Grant (SUNFUELS – Grant No. 320541) and ERC Starting Grant (TRIPOD – Grant No. 715132). We thank Patrick Basler, Thomas Cooper, Yago Gracia, Philipp Good, Gianluca Ambrosetti, Andrea Pedretti, David Rast, Max Schmitz, Nikolas Tzouganatos, and Michael Wild for their contributions to the technology development.

Author contributions: R.S, D.R., F.D., P.H., A.M, P.F. and A.S. designed the system's components; R.S., A.M. and D.R. executed the experiments; J.L. and A.P. performed the economic/policy analyses; P.F. and A.S managed and co-supervised the project; A.S. conceived the project idea and wrote the manuscript with input from all authors.

Competing Financial Interests: ETH Zurich has license agreements with its spinoff companies Climeworks and Synhelion, and owns the following patents: EP 09007467.5, WO2010/091831: Gebald, C., Wurzbacher, J., Steinfeld, A., Amine Containing Fibrous Structure for CO2 Capture; PCT/EP2014/001082: Steinfeld, A., Scheffe, J., Furler, P., Vogt, U., Gorbar, M., Open-cell materials for use in thermochemical fuel production processes; EP16194074, WO2018/073049: Steinfeld, A., Furler, P., Haselbacher, A., Geissbühler, L., A thermochemical reactor system for a temperature swing cyclic process with integrated heat recovery; EP18195213.68: Ackermann, S., Dieringer, P., Furler, P., Steinfeld, A., Bulfin, B., Process for the production of syngas. P.F. is the CTO of Synhelion; P.F and A.S. are shareholders of Synhelion.